Progress In Electromagnetics Research B, Vol. 89, 29–44, 2020

Reducing the Dimension of a Patch-Clamp to the Smallest Physical Limit Using a Coaxial Atom Probe

Pushpendra Singh[1, 2, *], Subrata Ghosh[3, 4], Pathik Sahoo[2], Kanad Ray[1], Daisuke Fujita[2], and Anirban Bandyopadhyay[2, *]

Abstract—For the last half a century, neurophysiology has relied on patch-clamp, which neutralizes the ions to sense a signal. The smaller the patch, the efficiency is better. However, the limit has not been reached yet, and we accomplish it here. We add a spiral and a ring antenna to a coaxial probe to significantly reduce its self-resonance when the tip filters the ultra-low vibrations of protein's sub-molecular parts (10^{-18} watts to 10^{-22} watts) in a living cell environment with 10^{-6}-watt noise. A probe tip added by a cavity resonator & a dielectric resonator acquires four distinct ultra-low noise signals simultaneously from a biomolecule, which is not possible using a patch-clamp. Protein transmits ions and small molecules. Our probe estimates the ionic content of the molecule. Simultaneously it also measures the dipolar oscillations of its sub-molecular parts that regulates ionic interaction. We experimentally measure signals over a wide frequency domain. In that frequency domain, we map the mechanical, electrical, and magnetic vibrations of the element and record the relationship between its electric and ionic conductions. Dimension wise it is the ultimate resolution, consistent both in silico & in real experiments with the neuron cells — the atomic pen instantly monitors a large number of dynamic molecular centers at a time.

1. INTRODUCTION

The coaxial probe is a bilayer electrode first used in 1987 to capture the reflection coefficient and permittivity of a dielectric material under high noise [1]. Since then, several versions of the coaxial probes have been used as a reliable sensor to instantly map a particular element mixed in a biomaterial [2], for the rapid & yet accurate diagnosis for point of care (POC). For example, measure the electromagnetic resonance of breast tissues for detecting diseases like cancer [3, 4], even it is used in the agricultural research [5] for detecting food adulteration, moisture content, etc. The coaxial probe has an additional shield to reduce the cross-talk between the neighboring electrodes. It can integrate multiple electrical responses simultaneously. Thus, one could explore its natural multiplexing ability. The coaxial electrode systems hold tremendous potential for a rapid, low cost yet highly sensitive biomarker detection platform. Nowadays, to learn diseases, an ELISA test is used, which requires sophisticated instruments; reagent consumption is high; multiplexing ability is low; and simultaneous detection of multiple infections is not possible. Coaxial probe fits to do all these operations in one, easy to use platform. Its applications could even be extended to study the fundamental & translational neuroscience by replacing the existing glass-made patch-clamp.

Received 24 July 2020, Accepted 15 September 2020, Scheduled 5 October 2020

* Corresponding author: Anirban Bandyopadhyay (anirban.bandyo@gmail.com), Pushpendra Singh (singhpushpendra548@gmail.com).

[1] Amity School of Applied Science, Amity University Rajasthan, Kant Kalwar, NH-11C, Jaipur Delhi Highway, Jaipur, Rajasthan 303007, India. [2] International Center for Materials and Nanoarchitectronics (MANA), Research Center for Advanced Measurement and Characterization (RCAMC), NIMS, 1-2-1 Sengen, Tsukuba, Ibaraki 3050047, Japan. [3] Chemical Science and Technology Division, CSIR-North East Institute of Science and Technology, NEIST, Jorhat, Assam 785006, India. [4] Academy of Scientific and Innovative Research (AcSIR), CSIR-NEIST Campus, Jorhat, Assam 785006, India.

Complex permittivity measurement is a specialty of coaxial probes due to its ability to measure phase and amplitude together [6]. It also fits to measure the electromagnetic radiation from the surfaces, which helps in measuring the energy exchange between nanomaterials [7]. Thus, coaxial probe has been a useful vibration sensor, even to read neuron signals. Current interests are growing in developing highly sensitive tools [8–13] for measuring the frequency tuning ability [14–19] of proteins and neurons, sub-threshold signals [18, 19] to learn brain's plasticity, and neurodegenerative diseases. The study would enhance manifold if the probes measure ultra-low-power cellular signals less than a few femto-watts (mV & pA $\sim 10^{-15}$ watts; pA = pico-ampere) or atto-watts (mV & fA $\sim 10^{-18}$ watts, fA = femto-ampere), to reach the energy level of a single protein vibration. However, the measurement should be much faster than the existing millisecond integration time [17, 18]. Contemporary biology primarily reports in the energy domain of $\sim 10^{-12}$ watts (mV and nA), relying only on the ionic & molecular signals resonating in the milliseconds time domain, — preferably optically, with a high integration time [19, 20]. However, we need a probe that can measure the protein or single-molecule vibration at a wide range of time scales, while operating at very low power sensing. Various techniques have been used to look into the sub-structures of cellular material below the optical limit [21, 22]. Our objective is to build a coaxial atomic probe that has universal applicability from medicine to food industry. A coaxial probe has already been proved efficient in sensing a layered biological medium [23] (Table 1), which does not require a high volume of protein solution [24], and its equivalent circuit is easy to model [25].

A coaxial probe has hardly been developed into a piece of state-of-the-art machinery [24–26]. When an additional metal layer covers a pure signal reading probe, a buffer potential between the probe-pairs is perturbed by the potential fluctuations of external noise. In the last 30 years of coaxial probe research, this is the only advantage that has been explored by tuning the probe dimension [1–7]. Temporal map of biosystems [27, 28] requires multi-mode use of coaxial probe [29–31], which we studied previously. However, no study was done on the theoretical understanding of the probe and its interaction with the biosystem under measurement. Here, we have underpinned three major theoretical advancements to enhance the basic sensing ability of a bilayer metal-semiconductor-metal platform

Table 1. A comparison between conventional nanotube-based patch-clamp and coaxial atom probe.

Patch Clamp	**Coaxial atom probe**
Captures ions from solution by physical charge neutralization.	No need to touch or neutralize the charge, wireless measure of ions.
Capture noise mixed-signal	Differential signal remove noise
Sense a narrow frequency band	Sense a wide frequency band
Detects only ions, cannot even distinguish ion types.	Wide ranges of materials could be detected using three probe frequencies.
Deforms nerve impulse due to the geometry of clamp shapes.	Geometry could be turned to sense a typical pulse.
Preamplifiers and lock-in amplifiers are all temporal filters.	Spatio-temporal filters take data as space and time difference.
It cannot sense ionic and molecular dynamics.	Change in phase and frequency detects symmetry breaking for various dynamics.
Statistical detection of the number of ions, an average relative to the probe.	Quantitative detection of symmetry and quantity of elements
Measures difference in ionic density between two places.	Resonates with a material matching phase, frequency, and emits energy as a burst.
Ion tube's inherent mechanical noise stops study inside a cell.	No tube to neutralize ions, repeated use possible, vibration doesn't break.

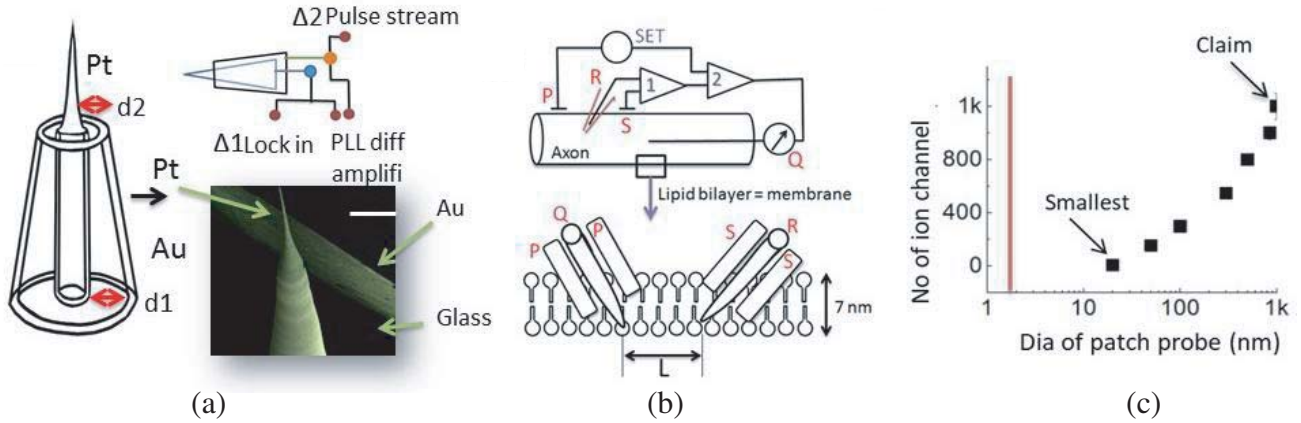

Figure 1. Measuring circuit using a coaxial probe & reduction of probe diameter: (a) Schematic of the coaxial electrode Au-glass-Pt system, ratio $d1/d2$ determines the actual sensing cavity between Au cover and Pt core. Signal from Au is commonly used to send pulse stream to sample ($\Delta 2$) if necessary, Pt core is used for a lock-in or filtering/amplifying the signal ($\Delta 1$). Phase-locked-loop (PLL) differential amplifier captures signal from the probe as ($\Delta 1$–$\Delta 2$). He-ion microscope image of a coaxial probe (scale bar 250 nm). (b) The top panel shows old methods for measuring the axonal membrane (lipid bilayer, 7 nm) using a patch-clamp glass tube or nanotube. The bottom panel shows measuring a lipid bilayer or membrane using two coaxial probes. L is the separation between two central Au probes of two coaxial electrodes. PQP mode measurement is replication of old method using coaxial probe, while SRS mode measurement is new circuit for using coaxial probe. (c) Curve between the diameter of the patch probe and the number of ion channels that a patch clamp covers after clamping with the membrane. The black plot is smallest reported diameters taken from various patch-clamp reports that claims single ion channel measurement. The red line depicts an ideal clamp diameter for a true single ion channel measurement.

(Fig. 1(a)), rather than advancing the filtering electronics that several other groups [24–26] and we used to practice commonly [29–31].

Three primary changes in the operational modes are explored in this work (Table 1). First, while measuring a protein or single-molecule vibration using a coaxial probe, we optimize the electromagnetic (*em*) source and ground locations (Fig. 1). A proper choice of source and sink decides the effective geometric features of a probe best suited for sensing a protein signal. Therefore, we investigated the possibility of using the dielectric part as a solid resonating sensor and the cavity between metal electrodes as a signal trapping sensor. The advantage of using two electrodes as dual sensors at the tip is that the differential signal if captured provides high-resolution noise-free data. Second, we wanted to learn, whether to get the maximum sensitivity of the probe, do we have to make a smaller probe, for which we received a surprising answer. The dimension of the probe should topologically match with the edge geometry of the metal shields and pure signal capturing core. Therefore, even a large 20 nm wide tip could achieve an atomic resolution. Therefore, we advance the technology to a domain where a topological match between (i) the tip edge diameter, (ii) the cavity shape between a pair of metal shields, and (iii) the embedded dielectric geometry together regulates the sensitivity of the probe (Fig. 2). Third, an additional ring & a spiral antenna were added to eliminate the noise by creating an artificial electromagnetic field due to the interference of resonant emissions. With an added metal layer covering the central signal detection probe, the cavity in between metallic layers acts as a capacitor, so the capacitive noise-blocking feature turns active. Additionally, here we add inductive coil right at the tip edge while sensing an external signal. The advantage of inductive blocking is eliminating the ac noise. We have covered major conceptual advances here as a combination of theory and experiments, compared to our previous works [29–31].

2. THEORETICAL SIMULATION AND THE EXPERIMENTAL PROTOCOL

2.1. Design and Fabrication of a Coaxial Tip

All coaxial probes studied here have a central Pt wire and covered with a cylindrical tube of Au, as shown in Fig. 1(a). The fabrication process of the coaxial probes is available in the literature [1–7]. We independently took the Japanese patent of a coaxial array chip JP-5187804 in 2006. Naughton et al. in 2016 built their version of the coaxial array-based chip [26], US 2014/0329707 A1. Primarily, an atomically sharp scanning tunneling microscope (STM) or atomic force microscope (AFM) tips are made of Pt or Pt/Ir composite (Pt/Ir1:1 is stronger, does not break often). An insulating glass coat is grown around the Pt core. Finally, an Au layer is e-beam evaporated on the top of the glass layer, so we get the desired Au-glass-Pt structure. Our coaxial probe shown in Fig. 1(a) reads three distinct signals at a time: the first from the outer metal Au layer, the second from an inner atomic sharp needle of Pt, and the third from the gap between these two metals. The gap is either empty or filled with dielectric (glass is one of many choices). The central dielectric region between two probes could sense a signal as a dielectric resonator or cavity resonator by trapping the signals reflected or radiated from the surface [27, 28]. The complex permittivity of a sample is determined from the coaxial aperture's reflection coefficient, which is measured by a vector network analyzer (VNA). The schematic of the measurement setup with a coaxial probe is shown in Fig. 1(b).

2.2. Theoretical Simulation and in Silico Experiment on the Protein and Neuron

Using electromagnetic simulation software — Computer simulation technology (CST) dielectric resonance simulator, we built coaxial probe, membrane, proteins & even neuron cells, & simulated resonance frequencies. For building molecules, we used balls and sticks, for neurons and proteins *.stl 3D printing files were made from pdb, and we could directly load them in CST. We carried out '*in silico experiments*' in CST by connecting probes with the artificially built protein, membrane & the neuron cells, as shown in Figs. 1(a), (b). Since the probe location in a cultured neuron experiment is equal to the port location for resonance simulator in an in-silico experiment, we change the location of the port, the geometry of the tip, and associative elements with a probe. Specifically, for in-silico experiment, we (i) varied the location of the electromagnetic source and the sink (ground), thus defined the energy transmission path, (ii) varied the tip edge geometry and (iii) inserted various antennas covering the measuring sample & the coaxial probe.

In the coaxial probe, we keep Au shield intact and reduce the Pt tip edge diameter from mm to μm to nm scale, and it is 10^3 orders jump twice in the spatial scale (Fig. 2). For any signal to transmit, we need a source where the probing signal is pumped, and a drain where the transmitted signal drains to the ground. The source and drain reverse in the case of an ac signal; thus, often it is important for an ac signal, where we locate the source and the drain. The symmetry of the structure connecting the source and the drain determines the frequency shifts in a resonance band. The location of an electromagnetic (em) wave source and the sink were varied. We have studied three cases (i) a single Pt wire as the source, (ii) outer cylindrical Au as source and Pt as the ground wire, (iii) Pt wire as the source and the cylindrical Au as the ground. For each scale, four combinations of pumping the energy to the probe are studied. Comparing all the three cases, we find that when Pt and Au are both connected to the source and drain at 1 mm Pt edge, the probe is the most reliable and sensitive, because it has a sharp resonance peak. However, when we have 1 μm or 1 nm wide probe, then, it is better to pump Pt alone keeping the Au probe isolated. Below we describe the typical features that we have obtained while varying the Pt tip's edge diameter. Fig. 3(a) summarizes tip resonance frequency as a function of tip diameter.

Figure 2 further suggests that at certain frequencies when the outer Au metal electrode and internal Pt electrode are energized in phase together, there is no distinct sharp resonance, rather a phase wave flows from top to the tip edge. We should avoid the frequencies where probe and sample have common resonance frequencies. We show the enhancement of potential read by the probe, where a probe senses an electromagnetic signal in the frequency range 10^{-6} Hz to 10^{15} Hz, preferably in the THz domain. The cavity between a Pt metal needle and an Au metal cylinder traps (10^{-20} watt) ultra-low signals in its vicinity. The cavity's conical geometry amplifies that signal (3 kHz to 40 GHz), and the embedded dielectric resonator (glass) increases the Q factor ($\sim 10^5$) at all frequencies. Unlike the patch-clamp, an

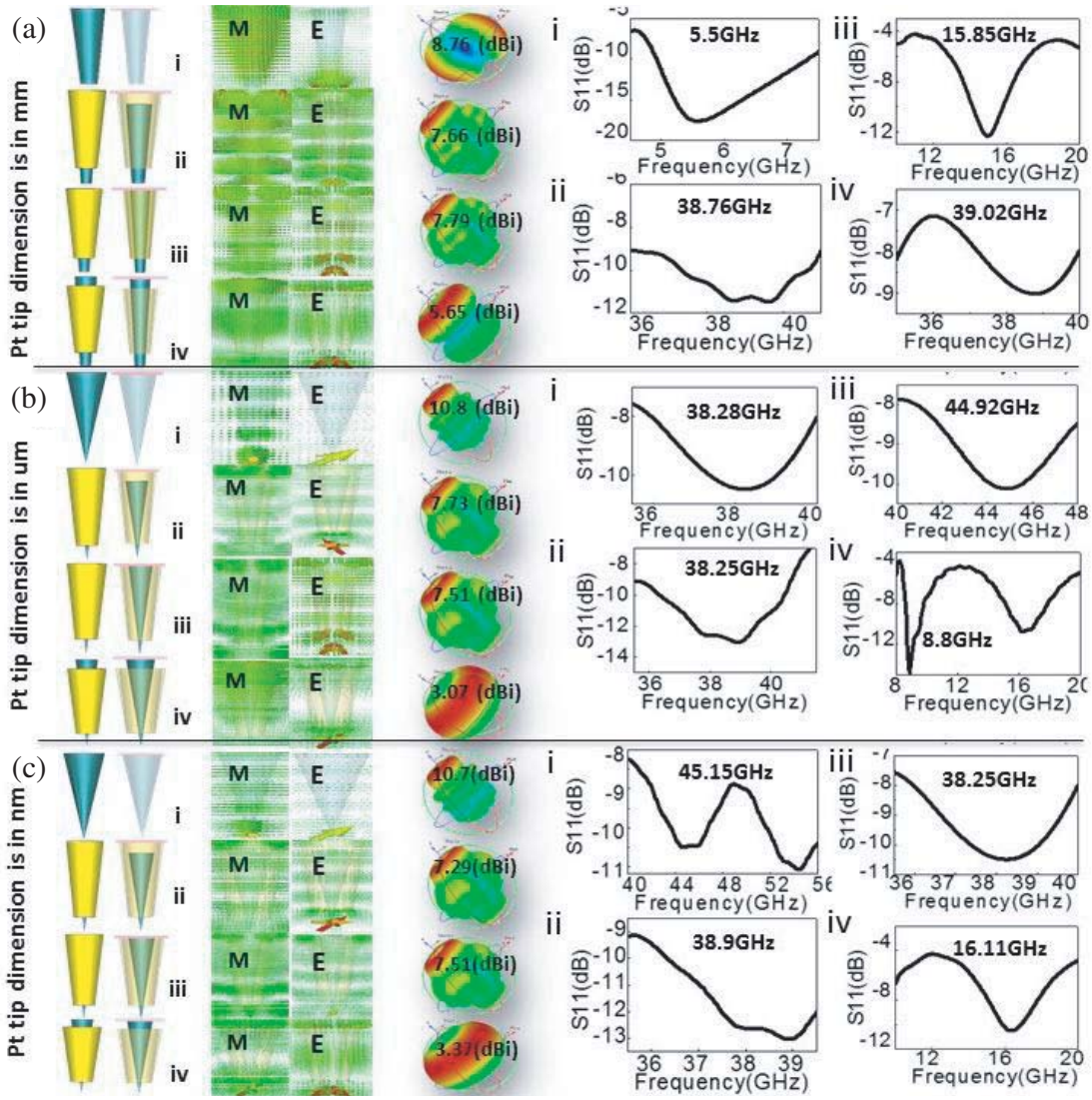

Figure 2. Geometric configuration optimization for Au-glass-Pt coaxial probe: CST simulator & time domain solver were used for all. **Column I** — Basic perspective view of co axial probe. **Column II** — The electric E and magnetic M fields are plotted at their resonance frequency. **Column III** — Directivity at resonance C**olumn IV** — Resonance peaks. Port location = top end of the device. Boundary condition = open space.

atom probe reads three signals at a time, filters signal from the noise with a ratio S/N $\sim 10^5$, measures four distinct vibrations of protein complexes, even deep inside a neuron membrane (7 nm). We used exact material parameters and dimensions using which the coaxial probe devices were built.

The details of fabrication and measurement circuits of a coaxial atom probe are reported [30], it is even used for imaging biological samples [31]. The atomic resolution coaxial probe could be used as a patch-clamp; at the same time, its dielectric resonator cavity would detect the protein vibrations [32–34] deep inside a live neuron cell [30, 31]. Apart from simulating the coaxial electrode, we have built an artificial neuron and tubulin protein model following accurate experimental details in CST (PDB structure was converted in CST), and studied their electromagnetic resonance properties theoretically [27]. For an atomic resolution setup, the tip-material junction's curvature dramatically changes the measurement scenario. The CST simulation described in Fig. 3 shows that if a membrane

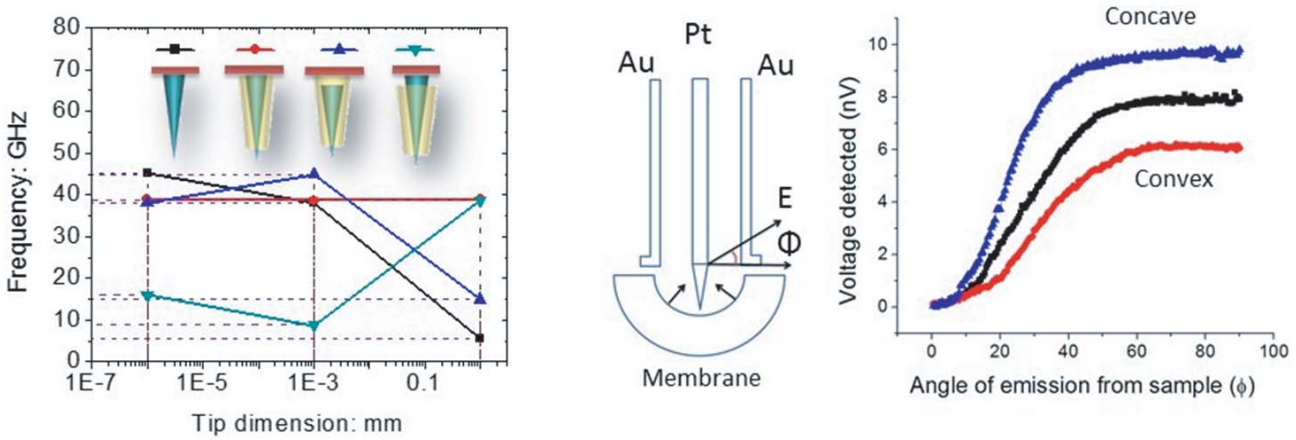

(a) (b)

Figure 3. Generic feature for probe response: Coaxial probe-membrane contact simulation: (a) A plot between frequency (GHz) and tip dimension (nm) for four configurations of coaxial atomic probes. (b). A schematic shows a piezo-motor driven insertion into the neuron membrane creates a concave surface (left). Electric field E emits at an angle ϕ from the biomaterial surface. CST simulated plots for the membrane-coaxial probe system for concave (blue), convex (red), flat (black) configurations of the membrane (right).

folds into a concave surface, the sample signal converges into a focal point (Fig. 3(b)). The sensitivity increases by 100%, while a convex surface diverges the emission or reflection from the surface (Fig. 3(b): right). The CST simulation of Fig. 1(a) shows that an optimized relative distance between a probe and the concave reflector delivers the maximum sensitivity. If the central tip Pt is far from the membrane, the Au electrode dominates. If very near, then the Pt signal dominates. Hence, we keep the tip in between.

Theoretical analysis of a coaxial probe suggests that the ratio of the two ends of our probe, the front-edge and rear-end diameters of a cavity resonator (ϵ is the dielectric constant of borosilicate glass), determines the pumping thrust and the sensing ability, $F = \frac{2P_0}{c} Q_u \left(\frac{\lambda_0}{d_1} - \frac{\lambda_0}{d_2}\right)\left(1 - \frac{\lambda_0^2}{\sqrt{\epsilon} d_1 d_2}\right)$ [35, 36]. It is Shawyer's thrust equation. The second term in the parenthesis is the relativistic correction term, here λ_0 is the wavelength of the detected signal. When a probe signal is pumped into the biomaterial, the transmitting power is focused due to the difference in edge diameters of the two metal electrodes coaxial probe. During sensing, the same topology enables the accumulation of a particular signal, and a subtle integration of signal enhances the sensing ability largely. The detection bandwidth of a coaxial probe is $\Delta f = f_2 - f_1$, and the limiting operational ratio is obtained from $\frac{d_2}{d_1} \approx \frac{f_1}{f_2}$. The current coaxial setup works as a fusion device. It is a sum of a dielectric resonator made of glass and a cavity resonator, which is an empty reflecting space between the Au cavity and the external surface of Pt. The self-resonance of the cavity of glass is given by $F = \frac{c}{2\pi\sqrt{\epsilon_r}} \sqrt{2\left(\frac{\pi}{d}\right)^2 + \left(\frac{\pi}{2l}\right)^2}$ [37]. One way of detecting resonance frequency is to measure the shift in the dielectric resonator's peak frequency when it is in contact with the biomaterial. The cylindrical cavity between the Au and Pt electrodes is also an additional detector. Due to the special design at the tip edge, a coaxial probe builds a filling cavity, encompassing the measuring biomaterial inside (Fig. 1(a)), so we accurately detect $\epsilon^{/} = \left(\frac{f_0}{f_s}\right)^2$, $\epsilon^{//} = \left(\frac{1}{Q_s} - \frac{1}{Q_0}\sqrt{\frac{f_0}{f_s}}\right)\left(\frac{f_0}{f_s}\right)^2$ [38], where $Q_0 = \frac{f_0}{f_0(3dB)}$, $Q_S = \frac{f_S}{f_S(3dB)}$. However, in some cases, during a measurement, the coaxial probe partially holds the biomaterial, then real and imaginary parts of the dielectric constants are $\epsilon^{/} = \frac{1}{2}\left(\frac{f_0}{f_s} - 1\right)\frac{V_e}{V_s} - 1$, and $\epsilon^{//} = \frac{1}{4}\left(\frac{1}{Q_s} - \frac{1}{Q_0}\right)\frac{V_e}{V_s}$. Due to the resonance of the biomaterial, the basic resonance frequency of the cavity changes from $f_0 \rightarrow f_s$ and the Q factor changes $Q_0 \rightarrow Q_s$. Thus, one detects biomaterials dielectric property as a change in phase and amplitude of its

dielectric constant. In summary, multiple modes act together in detecting resonance frequencies of a biomaterial, or coaxial electrode system has the multiplexing ability.

3. EXPERIMENTAL RESULTS AND DISCUSSIONS

3.1. Different Configuration Mode of Coaxial Atom Probe

The schematic of the coaxial probe used is shown in Fig. 1(a). It has two parts. One part is the central Pt metal wire, whose front edge is made sharp. Except for the front edge, Pt wire is covered with a dielectric glass layer, sintering after dipping into a polymeric coat, and an insulator layer is grown. On top of the insulator layer, the Au layer is vacuum evaporated. We get the coaxial probe. Here d1 and d2 are two parameters that are regulated [31, 32]. To the right of the schematic of a coaxial probe, He-ion microscope image of a coaxial probe is shown. In this work, we present the resonance frequency of the Au-glass-Pt system as a single structure.

We purchased embryonic rat hippocampal neuron cells from Lonza Inc and followed their specified protocol to culture the neuron cells. Then we have cultured hippocampus neuron cell and deposited 1 nm tubulin protein on a HOPG substrate for the direct measurement of resonance frequencies using a signal source and a vector network analyzer, VNA up to 178 GHz [29]. Here, 8–10 days old neuron cells were used for measuring the vibrations of the membrane by locating the coaxial probes exactly at the location on the membrane so that the setup mimics the device simulated theoretically [30, 31]. Similarly, we dropcast the 1 nm solution of tubulin protein purchased from Cytoskeleton Inc. on the HOPG substrate for imaging and measuring the electromagnetic resonance [29].

Figure 4(a) shows simultaneous insertion of a coaxial probe and a patch clamp in measuring the signal processing across a neuron. We use multiple coaxial probes, and each probe is inserted into the neuron at a specific depth at a specific location. The electrodes at Soma (S), axonal branch (AB), and dendrimer (D) make contacts with the membrane, remain within the 7 nm width, and probes are located deep inside the neuron by making contact with the micro-neuro-filaments shown in Fig. 4(b) (left) and tubulin protein shown in Fig. 4(b) (right).

Figure 5 shows the automated insertion of a coaxial probe to make a precise contact with the membrane surface. During approach to membrane the current and voltage is carefully monitored in power mode. Measuring an ultralow-power (10^{-18} watts to 10^{-21} watts) requires reading a picoampere

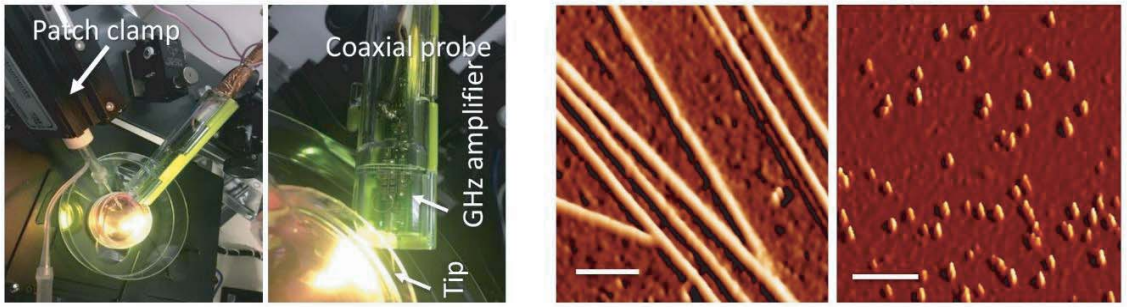

Figure 4. Coaxial probe and Patch-clamp are operating simultaneously on a single neuron: (a) Experimental set up for combined patch clamp and coaxial probe measurement on 8–10 days old hippocampal neuron in a cultured plate. The glass-tube of patch clamp is pressed with buffer solution to maintain pressure of the membrane-glass patch. The atomic resolution coaxial tip is connected to a GHz amplifier for instant signal amplification. Patch clamps sense only ion flows that resonates ~ 1 ms, read only one data at a time, cannot sense < 50–100 nm, but coaxial atom probe < 0.5 nm. Unlike patch clamp deep inside a neuron and atom probe filters noise (S/N $\sim 10^5$), measures four distinct vibrations of protein complexes. (b) Atomic force microscope, AFM images of microtubule (scale bar 120 nm), and tubulin protein (scale bar 130 nm) sample dried up by putting the substrate in the refrigerator for 2 hours.

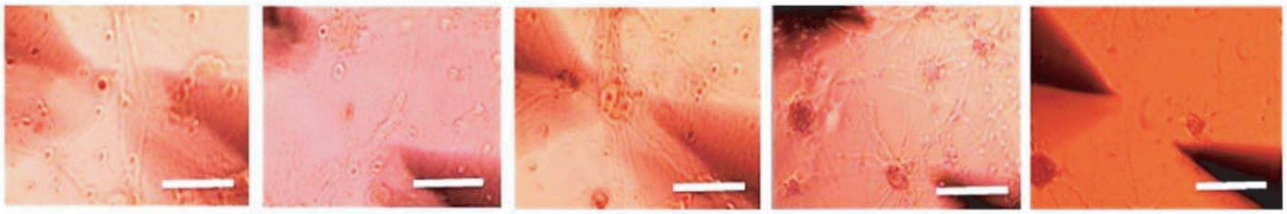

Figure 5. Time-lapse for coaxial probe approaches towards an axon: A image of a neuron, the probes are faded as the neuron, is focused. When the coaxial probe makes contact with the membrane in the last image, the electrodes appear focused (scale bar $\sim 100\,\mu$m).

range current (10^{-12} A) and a microvolt range voltage (10^{-6} V) that senses $\sim 10^{-18}$ watts. If the probe reads a femtoampere range current (10^{-15} A) and a microvolt range voltage (10^{-6} V), then it senses 10^{-21} watts. We do not primarily use nano voltmeter (10^{-9} V) as it slows down the rate of data acquisition and the voltage variation of proteins or single molecules. Organic molecules used in this study respond in between millivolt (10^{-3} V) and microvolt (10^{-6} V).

We compare two received signals from samples between the pair of electrodes Au and Pt, and acquire a differential signal (Figs. 6(a), (b)). A differential signal means that using an external ac signal source, a particular range of alternating sinusoidal wave is pumped into the sample, or a protein that is naturally vibrating. Then, two signals are captured from the sample. If the spatial separation between the probes is less than probe's field domain ($\sim 2\,\text{nm}^2$), then two probes Au and Pt capture the natural vibration or induced oscillations of a molecular system simultaneously. Then from the phase and amplitude differences between ac signals captured at two probes, the molecules' phase and amplitude are determined. In the conventional method, a lock-in amplifier is used; however, for the biological samples, lock-in amplifiers are not useful. A lock-in amplifier reads a pair of data for a given time interval and then takes the difference between the pair of signals captured; thus, it reduces the noise. If there is a larger fluctuation than signal due to noise, it autocorrects using programming encoded in

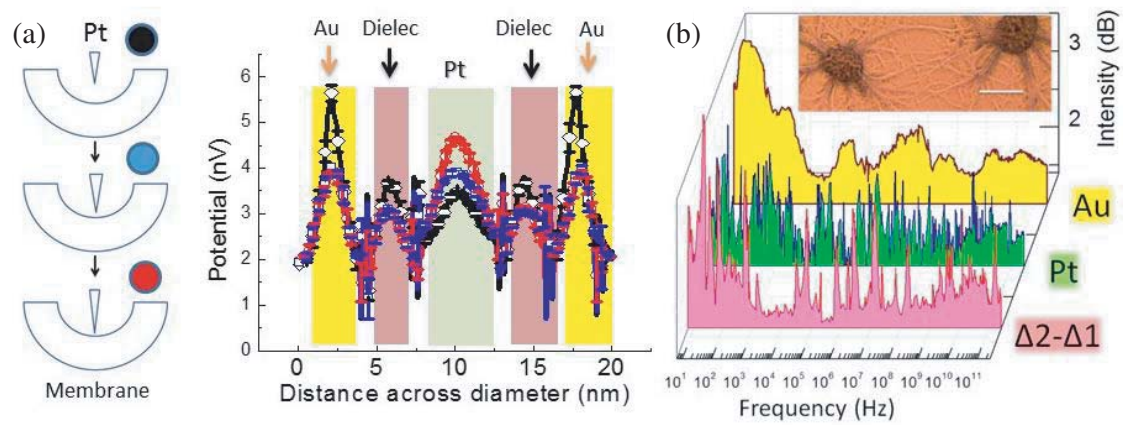

Figure 6. Theoretical and experimental measurement of neuron membrane: (a). Schematic of a Pt probe shifting the focal points in a concave membrane configuration (left). CST simulations for the three Pt-membrane curvature configurations (right). Far off, the focal point or membrane is a black line diamond symbol, at the focal point is a blue line with a square symbol, very close to the membrane, and off focal point is a red line with a circle symbol. (b). Three simultaneous measurements of coaxial probe connected to the neuron membrane; the microscopic image of neuron is in the inset (scale bar 80 μm). Three intensity vs. frequency plots in log scale are as follows. Pristine Au probe signal from the membrane is shaded yellow. Pristine Pt probe signal is shaded green (middle). The differential phase lock loop reading from pseudo energy levels is in the front (red line and shade).

it. In our case, two probes, operating in parallel, capture the same data from nearly the same points.

The method is conceptually different from a lock-in amplifier since a coaxial probe locks the signal both spatially and temporally. For this reason, a signal captured by our coaxial probe could be said as two coupled lock-in amplifiers capturing a signal at the atomic scale vicinity to acquire a difference of the differential signal. In Fig. 1(a), we show the electrode connections for Fig. 5 neuron image, used for Fig. 6 measurement. Here, the basic principle is the same. However, a common filtering point is kept for the synchronous measurement of all the probes at once. This experimental setup is essential for the current study, where we replicate the experimental setup in theory as similarly as possible.

The relative distance between the probes and the membrane regulates the folding of the membrane, as shown in Figs. 3(b) and 6(a). While making contact, balancing between the reflected light & movement of the motor holding the probe is required. Automated motions do not help much. One has to trust the relative contrast between probe and membrane, in the microscope as shown in a step by step contact-making process in Fig. 5. Once the automated piezo system naturally oscillates with the membrane, stable tip-membrane contact forms. The motion regulation & signal filtering algorithm follow CST simulation of a concave surface described in Fig. 6(a): left. The Fig. 6(b) shows an advantage of differential reading between an Au probe and a Pt probe. A frequency scan using an Au probe alone integrates the distinct resonance peaks, while the Pt electrode alone picks up even noises along with the sharp peaks. The differential signal between the probes $\Delta 1$–$\Delta 2$ delivers a highly sensitive resonance peak from the membrane (Fig. 6(b)). If either Au or Pt dominates, the recorded data are either masked or filled with false peaks, respectively. Then, we retract the tip by stopping the synchronous oscillation mode between tip and membrane and repeat the contact formation, which is an automated process similar to an STM operation.

While measuring membrane, protein or filaments like microtubule, if one makes contact with the water channel on their surface, then measured conductivity is several orders more than that if one contacts the surface [29]. In Fig. 7, we demonstrate a method to precisely control the water layer on biomaterials surface so that instead of surface water conduction we truly measure the biomaterial. Using a coaxial probe, we could image a single protein or any molecule and then set the tip at any location of the single-molecule and carry out the dielectric ac or dc measurement. Tubulin protein is a dimer, and we can see two high potential lobes in the tunneling current image, i.e., the localized density of states confines into two selected regions.

3.2. A Reliable Model of Coaxial Atom Probe

Atomically sharp Pt needle could be inserted half-way into the membrane, the intersection of the membrane's lipid bilayer or at any separation, by monitoring a rapid change in the current of the feedback loops (Fig. 6). The rate of change in the feedback currents while making a pair of contacts with the membrane needs an adjustment to minimize the current flow to less than 1–10 pA. The proper insertion between two lipid monolayers reduces noise dramatically in the 1 Hz to 178 GHz frequency response spectrum. We have described earlier [30], by clocking five probes on a neuron membrane and internal filamentary bundles of axon that multiple distinct signals flow in the filaments 250 µs before the growth of action potential [31]. Once we finish the membrane measurement, we enter the cytoskeleton.

Once the tip of coaxial probe is inserted, we begin automated hunt for desired biomaterials in the cytoskeleton. Protein hunt is not possible if a probe detects only one frequency, so we detect three frequencies and their associated phases simultaneously, using our coaxial probe. The motor moves back and forth to fine tune three frequencies. Driven by piezo motor and a coarse motor together as required, the coaxial atom probe moves in the cultured solution 2.5 ± 1 nm/minute resolution ($n = 400$). The change in the current profile is tracked in the Fig. 8 and is quantized. We use the coaxial atomic tip, namely Coat ($\sim 8 \pm 10\,\mathrm{M\Omega}$), or coaxial atomic patch clamp, Coapap ($\sim 120 \pm 10\,\mathrm{M\Omega}$), edge 0.1 nm, and the maximum exposed diameter varies between 2 nm and µm (rest insulated). In order to record the response for the 1 kHz to 20 GHz ac signals, different inductive (L), and capacitive (C) filters were used in the three axon core frequency bandwidth ranges (1 kHz–400 kHz, 3 MHz–400 Mz, 1 GHz–20 GHz) essentially to regulate the time constants (noise S/N $\sim 10^5$). The control electronics is elsewhere [29, 30], and its parameters were adjusted by connecting a matching preamplifier with the Coat and Coapap tips. The current profile for the atomic probe's penetration through the membrane (success $\sim 40\%$, $n = 400$; automatic approach time $\sim 20 \pm 2$ minutes) could confirm the contact material's resonance frequency

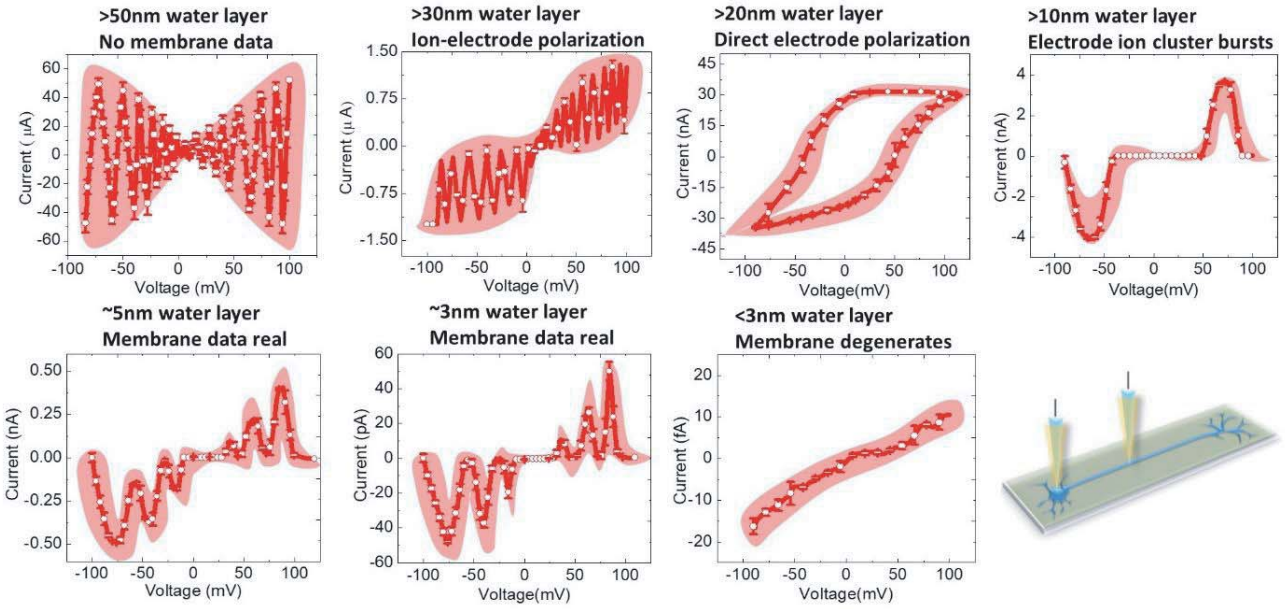

Figure 7. Current voltage characteristics on neuron membrane while de-ionisation for pure membrane measurement: Variation of feedback current while making a pair of contacts with the membrane. Culture solution around neuron membrane is replaced 20 minutes before the continuous seven sets of current voltage measurement carried out by a pair of coaxial probes (below threshold <90 mV) in a dehydration chamber. The scale bar of current changes significantly from μA to femto ampere, suggesting insertion of probe into the membrane and thus loss in conductivity between the pair of probes. The water content around the neuron membrane decreases from top to bottom, quartz crystal microbalance QCM method was used to find the z (zeta potential) oscillation profile of the water layer, thus, estimation of water content. A 2.5 nm–3 nm wide water layer is the best condition for protein (tubulin and microtubule here), but if this continues, the protein & lipid membrane undergoes an extreme stress during current voltage measurement, and the cell could even die. Experimental set up schematic is shown to the right.

triplet (microtubule $\sim$ 12 MHz, 22 MHz, 228 MHz; actin $\sim$ 75 kHz, 802 kHz, 335 MHz, 950 MHz; beta spectrin $\sim$ 120 kHz, 88 MHz, 97 MHz; Ancyrin $G \sim$ 870 MHz, 2.8 GHz, 180 GHz).

3.3. Coaxial Atom Probe with Various Pt-Au-Dielectric Configurations

Coaxial probes alone are not enough for precise vibrational spectroscopy in the noisy living cells or biological environments. The GHz noise source is connected to the probe, to carry out the simulation of noisy condition during real measurement. Better coaxial probe means a sharper resonance peak and a higher Q value. Figs. 9(a)–(e) show five plots side by side where the source of noise is varied to find how to carry out a credible measurement. These five figures show the structures of simulated coaxial devices, electric field E and magnetic field M distributions on the surface of the probe, resonance band plotted as intensity vs frequency, and to the extreme right the directivity plot, where on the surface of a sphere that accounts for all directions, the intensity of electromagnetic energy is mapped. During the simulation, a wild search was carried out to find the most prominent frequency domain of resonance, and a particular case is plotted here. Apart from the directivity of electromagnetic emission by the probe, we plot electric and magnetic fields distributions separately for all the cases because it is essential for building a proper tip to have a nearly similar distribution of the electric and magnetic fields. In certain cases, if either electric or magnetic field increases asymmetrically over the other, then it adds a nonlinear feature in the electromagnetic resonance pattern of the measuring device (Figs. 9(a)–(e)).

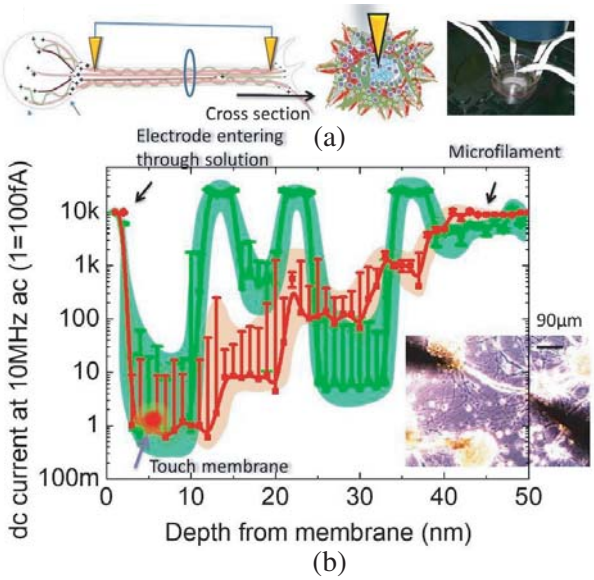

Figure 8. Hunt for a desired biomaterial inside a living cell using coaxial probe: (a) Schematic diagram showing the basic concept of a "protein hunt." "Protein hunt" is a search for a particular protein inside a living neuron cell. In panel (b), the current is in femto-ampere, but $1 = 100$ fA, means, when one reads current, multiply by 100fA. One microtubule transmits 1pA current, here, 1nA current comes from several microtubules, actins & neurofilaments constituting a bundle, and that is why conductivity is 10^3 times larger. (b) The plot is from Ghosh et al. 2016 [30]. The brown plot is a typical measurement when until the tip reaches very deep, we do not contact microtubule. The green plot is when the tip is inserted into Soma. When the tip touches the cytoskeleton, we see a jump in the current. Note that after contacts are made, the ultrasound vibrations to generate a virtual ground is switched off.

3.4. Coaxial Atom Probe with a Wrapped Spiral Ring

Furthermore, for reducing the self-resonance of the system and enabling it to capture the UV signal, we added (both electrodes are excited together) a spiral and a ring antenna as shown in Figs. 9(a)–(e). Sharper and accurate peaks are obtained by putting the extra rings surrounding the spiral antenna. Further improvement in sensitivity was observed when we added an extra metallic plate to the bottom of the substrate. The electromagnetic field distribution was confined at various locations of the coaxial probe system, to find the role of clusters of fields, in multiple setups, we checked all four parameters of S_{11}, S_{12}, S_{21}, and S_{22} (12 or 21 means transmission; 11 or 22 means reflection). The detailed description of simulated results with multiple ports (it means multiple waveguides as power supply) is reported in Figs. 9(a)–(e).

The significant difference between the probe signal sent to the sample and the detected reflection from the sample argues that a noise would be significantly reduced for Fig. 9(e) setup. So, it is extremely useful and the best device configuration. The wrapped ring of a coaxial atom probe reduces the self-resonance of electrode/connected source. Extra wrapped winding ring is proficient to make the sharpness of resonance frequency, increasing the Q value, while an extra metal sheet enables it to reduce the noise further while measuring the device resonance.

3.5. Simulated and Experimentally Signal Detection inside Living Cells (Neuron and Tubulin Protein)

We varied the geometry of the tip edge and the location of the *em* source in Fig. 2. Then, we improved the antenna network all around the coaxial probe (Fig. 9). Finally, by inserting multiple distinct antennas into a single sample, we have simulated the resonance bands, directivity of emitted field, and the electric

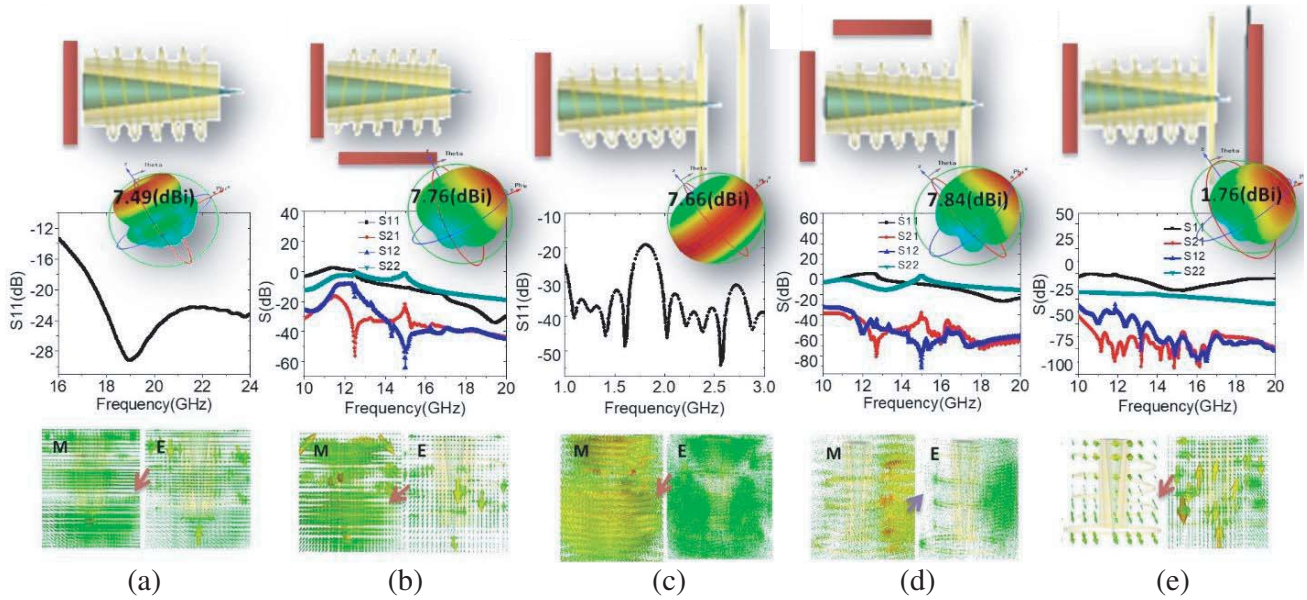

Figure 9. Five electrode configurations and theoretical simulation of probe adjacent below: (a) Wrapped ring probe with port1; (b) wrapped ring probes with one additional port2 at the side of the wrapped ring; (c) probes with two additional different diameter rings, one small diameter's ring at the tip of Pt wire while another ring at below of Pt tip edge; (d) wrapped ring setup mode with one ring around at Pt tip and put additional port2 at the wrapped ring; (e) The same setup mode of probe-like as case-d except for one metallic sheet below of Pt tip edge by putting port1 at both electrodes (Au & Pt) and port2 at the metallic plate. **Simulation detail.** Used software — CST; Used solver = Time domain solver; Port location = port1 at top end and port2 at one side of the device; Boundary condition = open space. Waveguide port, WGP; Resonance frequency, RF; Port dimension, PD. a WGP = $7.8 \times 7.8\,\mathrm{mm}^2$, RF = 18.96 GHz. **b.** WGP = $7.8 \times 7.8\,\mathrm{mm}^2$ (port1), $10 \times 17\,\mathrm{mm}^2$ (port2). RF = 15 GHz; c WGP = $7.8 \times 7.8\,\mathrm{mm}^2$. RF = 15 GHz. d WGP = $7.8 \times 7.8\,\mathrm{mm}^2$ (port1), $10 \times 17\,\mathrm{mm}^2$ (port2). RF = 12.7 GHz; e PD = $8.2 \times 8.2\,\mathrm{mm}^2$, RF = 12.5 GHz.

and magnetic field distributions on the materials surface (Fig. 10). In the conventional resonance band simulation, the probe is always invisible. It means that the effect of the probes is not considered in the calculation of the resonance frequencies. Here, we put the probes such that the entire system works as a singular system. All elements resonate together. Thus, we largely replicate the experimental situation practically in theory. Sharpness of the Pt needle is a concern. In 1979 when it was first proposed that if needle is sharpened to a single atom tip, it measures the tunneling current. The finding later led to the invention of a scanning tunneling microscope (STM). Argument for STM was that for dc signal "smaller tip delivers a better resolution". However, for an ac signal, the magnitude of wavelength interacts with tip, thus, regulates temporal and spatial resolutions for data acquisition.

One to one correspondence between experimentally and theoretically determined S_{11} for neuron and tubulin is shown in Fig. 10. We could simulate the electromagnetic resonance properties by creating a look-alike model of the real cultured neuron in the CST simulator and replicate the entire experiment [27]. The resonance frequencies approximately match between theory and experiment at 2.8 THz, 6 THz, 9 THz, 12 THz, 15 THz and 2.2 THz, 5.02 THz, 9.8 THz, 11 THz, 17.5 THz between mid panel and right panel in Fig. 10(a), respectively. The mismatch is 0.5 THz maximum. Similarly, in Fig. 10(b), theoretical and experimental resonances peaks correspond to each other at 4.25 GHz and 4.71 GHz frequencies. Mismatch is 0.4 THz maximum.

Here, instead of one probe to a neuron, we used multiple piezo motors to operate various different probes simultaneously to precisely placing them into the neuron. We have carried out three kinds of measurements on 8–10 days old hippocampus neurons. Fig. 10(a): left is three specific neuron measurement setups that have been theoretically simulated for the S_{11} measurements, as shown

in Fig. 10(a): middle, and the experimental measurements are shown in Fig. 10(c): right. Here, Fig. 10(a)(i) is a setup where no electrodes are added to the neuron. We get pure resonance behaviors of the neuron membrane. Then, we place the probes inside the Soma. Both electric and magnetic field distributions are focused on the soma region, but energy does not exchange with the axonal branches (Fig. 10(a)(ii)). We thought that this surprising result is an artifact. However, by putting more than one probe, a similar outcome was observed, i.e., all input energy canalizes to Soma (Fig. 10(a)(iii)). The experimental data for each case, i.e., internal signal transmission in the neuron, are shown in Fig. 10(a), right. A comparison of the simulated and experimental resonance bands for each case is depicted in Fig. 10(a), middle and right panels, respectively. It shows a significant resemblance between theory and experiment. The resonance peaks for both experiment and theory primarily overlap ($\sim 60\%$) at the same frequencies in the THz domain.

For tubulin, we repeated the simulation without (Fig. 10(b)(i)) and with the probe (Fig. 10(b)(ii)). The signs of energy exchanges are observed in different local parts of the tubulin protein, i.e., the cluster of α helices, i.e., sub-structure of protein or groups of secondary structures of the protein. Most importantly, we find that even if we connect the coaxial probes with the single tubulin protein, the distributions of electric and magnetic fields remain identical. The observation suggests that the measurements do not capture noisy peaks as real ones, just like the neuron measurement. The successful

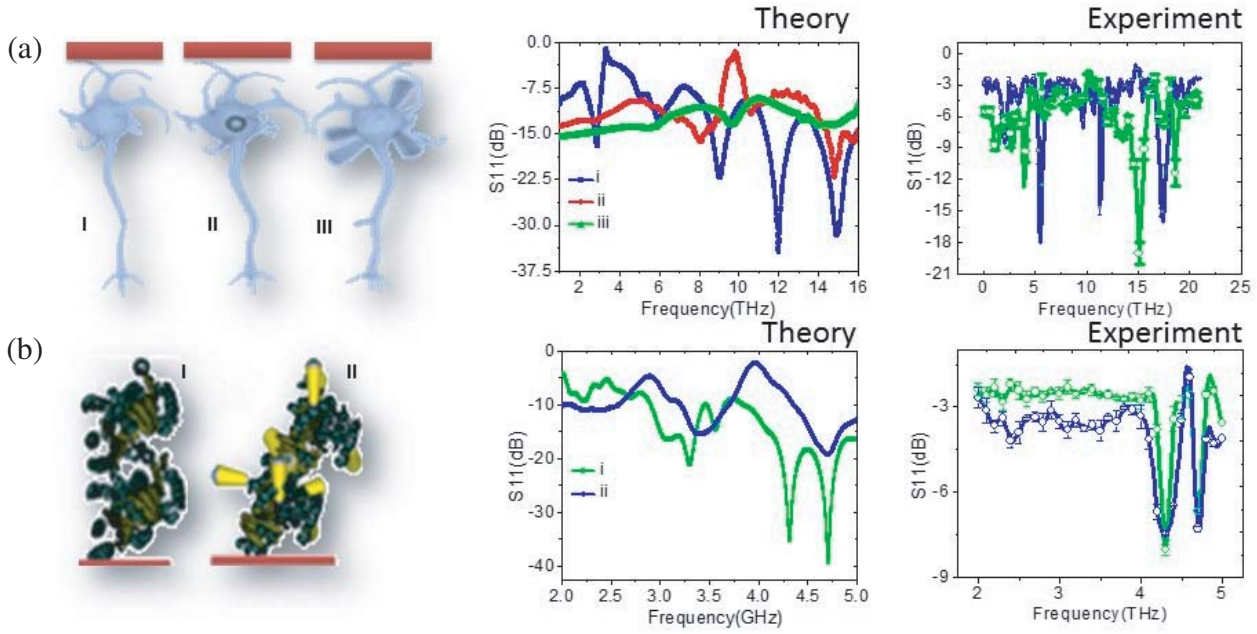

Figure 10. One to one correspondence between experimental and theoretical measurement of neuron and single protein. (a). Three neuron measuring devices in CST are shown (I, II, III). Four probes are placed inside the neuron and one on the neuron membrane. Probes are wrapped with *an inductive spiral + rings with two different diameters + one metallic cover*. The neuron is excited by putting a single probe (II) and several probes (III) around the soma region. Simulated and experimental resonance curves are depicted in the middle and right panels, respectively. The color code for middle and right are kept the same. (b) Tubulin simulation: when tubulin simulation without probe and tubulin energized by several coaxial atom probes. Simulated and experimental resonance curves for both the case are shown in middle and right panel, respectively, I (green), II (blue). **Simulation detail**. Used software — CST; Used solver = Time domain solver; Boundary condition = open space. Waveguide port, WGP; Resonance frequency, RF; Port dimension, PD. For panel (a) I, II & III: For ports attached at axonal branches; WGP $= 4.5e+004 \times 4.0e+004\,\mathrm{nm}^2$; RF for I, II & III = 9.06 THz, 2.86 THz, 2665.9 GHz. For panel (**b**), tubulin simulation; Port at one sub-tubuline (α and β) of tubulin, WGP $= 0.6e+005 \times 0.6e+005\,\mathrm{nm}^2$; RF for case I & II in Fig. (b) = 4.2 THz, 2.85 THz.

transfer of energy between one sub-tubulin to another sub-tubulin within a single molecule through the beta sheets and the consistent connectivity between the local functional groups could be studied in detail by recording the signals via multiple atom probes simultaneously. The experimental result of tubulin's density of states is depicted in Fig. 10(b), right. The field distribution is restricted in a single sub-tubulin in the absence of the probes. Similar resonance peaks are detected experimentally, which comprehensively resemble the simulated ones in Fig. 10(b), middle. A significant sharp peak and a band of weak oscillatory peaks show that the detection of resonance frequencies is practically possible with a very high Q value.

4. CONCLUSION

Existing patch-clamp uses a glass tube that cannot be reduced to the molecular scale. In contrast, when a coaxial probe is reduced to the molecular scale, the nano-scale ion neutralization at metallic tip-edge defects is rapid. For that reason, even after reaching the smallest physical limit, a coaxial probe provides superior performance. Ion neutralization sends a burst in the differential signal between Au and Pt. Our study identifies the unexplored potentials of a little modified coaxial probe. The probe can detect instantly if a molecule changes its conformation, e.g., a protein misfolds in disease, by dipping it in a solution. A user has to put the atom probe inside a winding spiral and covers the gap between the substrate and the Pt tip with a ring antenna. The fusion of inductive and capacitive filtering at the tip not only reduces the external noise, but also amplifies the contributions of the measuring system. It has been demanded over and over for the last half a century that for measuring the internal signal inside a single molecule, we have to decrease the resonance peaks from measuring systems. In that respect, the cell membrane reflects most parts of the shined electromagnetic wave, and only a selected few frequencies are filtered into the cytoskeleton and filaments. Several filamentary nanowires like microtubule, actin, and neurofilaments beat inside in the fluid and leave their signatures on the membrane. Moreover, the detection of micro-neurofilament resonance peaks on the vibrating membrane was never reported before and after a firing. It suggests that the cell fluid or cytoskeleton is not silent. Our atomic probe could sense subtle electromagnetic bursts, signals, and phase change in the systems that operate at most six time-scales at a time. Most importantly, our experimental measurements of a single molecule like DNA, carbon nanotube, chlorophyll, tubulin protein, *in vitro*, microfilaments in the neuron, and the neural membrane deliver a reliable consistency between theory & experiment. That is the primary advancement in the current study compared to our previous studies on the coaxial probe [29–31]. Therefore, we could ascertain that the fundamental changes in measuring with a coaxial probe are essential to be brought in the day-to-day measurements of the dielectric property in the food and medical industry.

ACKNOWLEDGMENT

Authors acknowledge the Asian office of Aerospace R&D (AOARD) a part of the United States Air Force (USAF), for grant No. FA2386-16-1-0003 (2016-2019) on electromagnetic resonance-based communication and intelligence of biomaterials.

REFERENCES

1. Marsland, T. P. and E. Evans, "Dielectric measurements with an open-ended coaxial probe," *IEEE Proceedings H — Microwaves, Antennas and Propagation*, Vol. 134, 341–349, 1987.
2. Meaney, P. M., B. B. Williams, S. D. Geimer, A. B. Flood, and H. M. Swartz, "A coaxial dielectric probe technique for distinguishing tooth enamel from dental resin," *Adv. Biomed. Eng. Res.*, Vol. 3, 8–17, 2015.
3. Hagl, D. M., D. Popovic, S. C. Hagness, J. H. Booske, and M. Okoniewski, "Sensing volume of open-ended coaxial probes for dielectric characterization of breast tissue at microwave frequencies," *IEEE Transactions on Microwave Theory and Techniques*, Vol. 51, 1194–1206, 2003.

4. Lazebnik, M., D. Popovic, L. McCartney, C. B. Watkins, M. J. Lindstrom, J. Harter, S. Sewall, T. Ogilvie, A. Magliocco, T. M. Breslin, W. Temple, D. Mew, J. H. Booske, M. Okoniewski, and S. C. Hagness, "A large-scale study of the ultrawideband microwave dielectric properties of normal, benign and malignant breast tissues obtained from cancer surgeries," *Physics in Medicine and Biology*, Vol. 52, 6093–6115, 2007.
5. SheenI, N. I. and M. Woodhead, "An open-ended coaxial probe for broad-band permittivity measurement of agricultural products," *J. of Agricult. Eng. Res.*, Vol. 74, 193–202, 1999.
6. Grant, J. P., R. N. Clarke, G. T. Symm, and N. M. Spyrou, "A critical study of the open-ended coaxial line sensor technique for RF and microwave complex permittivity measurements," *J. Phys. E Sci. Instrum.*, Vol. 22, 757–770, 1989.
7. Baudry, D., A. Louis, and B. Mazari, "Characterization of the open ended coaxial probe used for near-field measurements in EMC applications," *Progress In Electromagnetics Research*, Vol. 60, 311–333, 2006.
8. Goodman, M. B. and S. R. Lockery, "Pressure polishing: a method for reshaping patch pipettes during fire polishing," *J. Neurosci. Methods*, Vol. 100, 13–15, 2000.
9. Novak, P., J. Gorelik, U. Vivekananda, A. I. Shevchuk, Y. S. Ermolyuk, R. J. Bailey, A. J. Bushby, G. W. J. Moss, D. A. Rusakov, D. Klenerman, D. M. Kullmann, K. E. Volynski, and Y. E. Korchev, "Nanoscale targeted Patch-clamp recordings of functional presynaptic ion channels," *Neuron*, Vol. 79, 1067–1077, 2013.
10. Kodandaramaiah, S. B., G. T. Franzesi, B. Y. Chow, E. S. Boyden, and C. R. Forest, "Automated whole-cell patch-clamp electrophysiology of neurons in vivo," *Nature Methods*, Vol. 9, 585–587, 2012.
11. Zhao, Z., L. Luan, X. Wei, H. Zhu, X. Li, S. Lin, J. J. Siegel, R. A. Chitwood, and C. Xie, "Nanoelectronic coating enabled versatile multifunctional neural probes," *Nano Lett.*, Vol. 17, 4588–4595, 2017.
12. Gonzales, D. L., K. N. Badhiwala, D. G. Vercosa, B. W. Avants, Z. Liu, W. Zhong, and J. T. Robinson, "Scalable electrophysiology in intact small animals with nanoscale suspended electrode arrays," *Nat. Nanotech.*, Vol. 12, 684–691, 2017.
13. Schuhmann T. G. J., J. Yao, G. Hong, T. M. Fu, and C. M. Lieber, "Syringe-injectable electronics with a plug-and-play input/output interface," *Nano Lett.*, Vol. 17, 5836–5842, 2017.
14. Azevedo, A. W. and R. I. Wilson, "Active mechanisms of vibration encoding and frequency filtering in central mechanosensory neurons," *Neuron*, Vol. 96, 1–15, 2017.
15. Hudspeth, A. J. and R.S. Lewis, "A model for electrical resonance and frequency tuning in saccular hair cells of the bull-frog, Rana catesbeiana," *J. Physiol.* Vol. 400, 275–297, 1988.
16. Hutcheon, B. and Y. Yarom, "Resonance, oscillation and the intrinsic frequency preferences of neurons," *Trends Neurosci.*, Vol. 23, 216–222, 2000.
17. Lundstrom, B. N., M. Famulare, L. B. Sorensen, W. J. Spain, and A. L. Fairhall, "Sensitivity of firing rate to input fluctuations depends on time scale separation between fast and slow variables in single neurons," *J. Comput. Neurosci.*, Vol. 27, 277–290, 2009.
18. Ratte, S., M. Lankarany, Y. A. Rho, A. Patterson, and S. A. Prescott, "Subthreshold membrane currents confer distinct tuning properties that enable neurons to encode the integral or derivative of their input," *Front. Cell. Neurosci.*, Vol. 8, No. 452, 1–15, 2015.
19. Jin, L., Z. Han, J. Platisa, J. R. Wooltorton, L. B. Cohen, and V. A. Pieribone, "Single action potentials and subthreshold electrical events imaged in neurons with a fluorescent protein voltage probe," *Neuron*, Vol. 75, 779–785, 2012.
20. Akemann, W., H. Mutoh, A. Perron, J. Rossier, and T. Knöpfel, "Imaging brain electric signals with genetically targeted voltage-sensitive fluorescent proteins," *Nat. Methods*, Vol. 7, 643–649, 1020.
21. Maheswari U., H. Tatsumi, Y. Katayama, and M. Ohtsua, "Observation of subcellular nanostructure of single neurons with an illumination mode photon scanning tunneling microscope," *Optics Communications*, Vol. 120, 325–334, 1995.

22. Wang, Y., H. Fathali, D. Mishra, T. Olsson, J. D. Keighron, K. P. Skibicka, and A.-S. Cans, "Counting the number of glutamate molecules in single synaptic vesicles," *J. Am. Chem. Soc.*, Vol. 141, 44, 17507–17511, 2019.
23. Alanen, E., T. Lahtinen, and J. Nuutinen, "Variational formulation of open-ended coaxial line in contact with layered biological medium," *IEEE Trans. on Biomed. Eng.*, Vol. 45, 1241–1248, 1998.
24. Meaney, P. M., A. Gregory, N. Epstein, and K. D. Paulsen, "Microwave open-ended coaxial dielectric probe: interpretation of the sensing volume revisited," *BMC Med. Phys.*, Vol. 14, 1756–6649, 2014.
25. Liao, K., Y. Wu, C. Qian, and G. Du, "An accurate equivalent circuit method of open ended coaxial probe for measuring the permittivity of materials," X. Wan (eds)., *Electrical Power Systems and Computer, LNEE*, Springer, Berlin, Heidelberg, 2011.
26. Naughton, J. R., T. Connolly, J. A. Varela, J. Lundberg, M. J. Burns, T. C. Chiles, J. P. Christianson, and M. J. Naughton, "Shielded coaxial optrode arrays for neurophysiology," *Front Neurosci.*, Vol. 10, 252, 2016.
27. Singh, P., et al., "A self-operating time crystal model of the human brain: Can we replace entire brain hardware with a 3D fractal architecture of clocks alone?" *Information*, Vol. 11, No. 5, 238, 2020.
28. Bandyopadhyay, A., "Chapter 7-A complete, integrated time crystal model of a human brain," *Nanobrain. The Making of an Artificial Brain from a Time Crystal*, 372, Taylor & Francis Inc. Imprint CRC Press Inc., Publication City/Country Bosa Roca, United States, 2020.
29. Saxena K., et al., "Fractal, scale free electromagnetic resonance of a single brain extracted microtubule nanowire, a single tubulin protein and a single neuron," *Fractal Fract*, Vol. 4, No. 2, 11, 2020.
30. Ghosh, S. S. Sahu, L. Agrawal, T. Shiga, and A. Bandyopadhyay, "Inventing a coaxial atomic resolution patch clamp to study a single resonating protein complex and ultra-low power communication deep inside a living neuron cell," *J. Int. Neurosci.*, Vol. 15, 403–433, 2016.
31. Agrawal, L., S. Sahu, S. Ghosh, T. Shiga, D. Fujita, and A. Bandyopadhyay, "Inventing atomic resolution scanning dielectric microscopy to see a single protein complex operation live at resonance in a neuron without touching or adulterating the cell," *J. Int. Neurosci.*, Vol. 15, 435–462, 2016.
32. Sahu, S., S. Ghosh, D. Fujita, and A. Bandyopadhyay, "Live visualizations of single isolated tubulin protein self-assembly via tunneling current: effect of electromagnetic pumping during spontaneous growth of microtubule," *Sci. Rep.*, Vol. 4, No. 7303, 1–9, 2014.
33. Sahu, S., S. Ghosh, K. Hirata, D. Fujita, and A. Bandyopadhyay, "Multi-level memory switching properties of a single brain microtubule," *Appl. Phys. Lett.*, Vol. 102, No. 123701, 1–4, 2013.
34. Sahu, S., S. Ghosh, B. Ghosh, K. Aswani, K. Hirata, D. Fujita, and A. Bandyopadhyay, "Atomic water channel controlling remarkable properties of a single brain microtubule: Correlating single protein to its supramolecular assembly," *Biosensors and Bioelectronics*, Vol. 47, 141–148, 2013.
35. Dan, Ye., L. Jun, and T. Jau, "Jet propulsion by microwave air plasma in the atomosphere," *AIP Advances*, Vol. 10, 055002, 2020.
36. Jaun, Y., et al., "Prediction and experimental measurement of the electromagnetic thrust generated by a microwave thruster system," *Chinese Physics B*, Vol. 22, No. 5, 050301, 2013.
37. Yaduvanshi, R. S. and H. Parthasarathy, "Chapter 1-rectangular DRA fundamental background-rectangular dielectric resonator antenna — theory and design," *Springer*, New Delhi, Heidelberg, New York, Dordrecht, London, 2016.
38. Behagi, A. A., "Chapter 4: Resonant circuits and filters — RF and microwave circuit design: A design approch using (ADS), advanced design system," *Techno Search*, 2015.